Appl. Math. Mech. -Engl. Ed., **45**(3), 479–496 (2024)

APPLIED MATHEMATICS AND MECHANICS (ENGLISH EDITION)

https://doi.org/10.1007/s10483-024-3086-9

Nonlinear dynamic modeling of planar moving Timoshenko beam considering non-rigid non-elastic axial effects*

M. ABBASI GAVARI, M. R. HOMAEINEZHAD†

Faculty of Mechanical Engineering, K. N. Toosi University of Technology, Tehran 19991-43344, Iran

(Received Oct. 17, 2023 / Revised Jan. 12, 2024)

Abstract Due to the importance of vibration effects on the functional accuracy of mechanical systems, this research aims to develop a precise model of a nonlinearly vibrating single-link mobile flexible manipulator. The manipulator consists of an elastic arm, a rotary motor, and a rigid carrier, and undergoes general in-plane rigid body motion along with elastic transverse deformation. To accurately model the elastic behavior, Timoshenko's beam theory is used to describe the flexible arm, which accounts for rotary inertia and shear deformation effects. By applying Newton's second law, the nonlinear governing equations of motion for the manipulator are derived as a coupled system of ordinary differential equations (ODEs) and partial differential equations (PDEs). Then, the assumed mode method (AMM) is used to solve this nonlinear system of governing equations with appropriate shape functions. The assumed modes can be obtained after solving the characteristic equation of a Timoshenko beam with clamped boundary conditions at one end and an attached mass/inertia at the other. In addition, the effect of the transverse vibration of the inextensible arm on its axial behavior is investigated. Despite the axial rigidity, the effect makes the rigid body dynamics invalid for the axial behavior of the arm. Finally, numerical simulations are conducted to evaluate the performance of the developed model, and the results are compared with those obtained by the finite element approach. The comparison confirms the validity of the proposed dynamic model for the system. According to the mentioned features, this model can be reliable for investigating the system's vibrational behavior and implementing vibration control algorithms.

Key words planar moving Timoshenko beam, non-rigid non-elastic axial effect, assumed mode method (AMM), nonlinear motion analysis

Chinese Library Classification O322, O241.8
2010 Mathematics Subject Classification 70J50, 35A35, 34B15, 65K10, 35Q74

1 Introduction

Recently, the use of elastic manipulators in industrial applications has grown significantly due to their lighter weight, higher energy efficiency, and higher payload-to-weight ratio compared with rigid manipulators[1]. In addition to the mentioned features, elastic arms are safer

* Citation: ABBASI GAVARI, M. and HOMAEINEZHAD, M. R. Nonlinear dynamic modeling of planar moving Timoshenko beam considering non-rigid non-elastic axial effects. *Applied Mathematics and Mechanics* (*English Edition*), **45**(3), 479–496 (2024) https://doi.org/10.1007/s10483-024-3086-9

† Corresponding author, E-mail: mrhomaeinezhad@kntu.ac.ir

to manipulate objects than rigid ones, making them increasingly developed in medicine, particularly in surgical grippers[2]. The application of axially moving piezoelectric nanobeams in self-powered components of biomedical nanorobots is another example of applying elastic elements in medical applications[3]. On the other hand, the need for relatively long arms in spacecraft[4] and space explorations[5] due to reduced bending stiffness and increased deformations is equivalent to using elastic manipulators. Despite the mentioned advantages, deformation and vibration are among the issues that can disrupt the performance of flexible manipulators. Usually, the accuracy of the tip point position and the velocity of manipulators is critical, which may be disturbed in the presence of vibration. Overcoming such defects may face difficulties because forces and torques are only available in joints, not at the tip points. This issue has motivated researchers to seek ways to reduce vibrations and increase the functional accuracy of flexible structures and manipulators through active[6] or passive[7] methods.

In general, robotic arms are modeled using beam governing theories because one of their dimensions (axial direction) is much larger than the others. For Hookean materials, with the assumption of small rotation angles, geometric and neutral axes coincidence, perpendicularity of sections to the neutral axis after deformation, and ignoring Poisson's effect, four well-known models, i.e., the Euler-Bernoulli[8], Rayleigh[9], shear[10], and Timoshenko beam models, were presented[11]. The Euler-Bernoulli theory has been dominantly used among the mentioned models due to its more straightforward structure and better predictions for beams with large slenderness ratios[12]. However, experimental tests have shown that the most accurate predictions among the four mentioned theories is Timoshenko's approach because of its complete configuration[13].

Modeling a continuous system such as a beam will result in partial differential equations (PDEs) and several boundary conditions. The resulting PDEs will have analytical solutions only under particular conditions. However, even if the theory used for the continuous system is linear, due to the nonlinear geometry or special boundary conditions, it may be impossible to solve the resulting PDEs using analytical methods. For this reason, reduced-order modeling techniques, such as the assumed mode method (AMM), the finite difference method (FDM), the finite element method (FEM), the lumped parameters method (LPM), and the differential quadrature method (DQM), have been used to solve the governing equations of continuous systems[12,14].

The dynamical model of single-link robotic manipulators has been widely used in research related to vibration control. The mechanical arm was often mounted on a rotating base, and its translational motion was not considered. A significant percentage of the manipulators have been modeled using the Euler-Bernoulli theory[15–16], while models based on Timoshenko's approach[17–18] were relatively rare. The reduced-order modeling methods commonly used in these studies include the AMM, FDM, FEM, and LPM.

By reviewing related references, a limited number of studies have addressed the issue of flexible mobile manipulators. A vibration analysis of a Timoshenko beam clamped to a moving base has been studied in Ref. [19]. The study focused on extracting natural frequencies and mode shapes of a Timoshenko beam with a tip payload located vertically on a moving base. In Refs. [20]–[21], the vibration control of a moving vehicle-mounted flexible manipulator was studied. The dynamical modeling and vibrational behavior assessment of a soft-link underwater manipulator on a rigid vehicle were investigated in Ref. [22]. In Ref. [23], the dynamical modeling of a mobile manipulator with viscoelastic links and revolute-prismatic joints was considered. Lastly, another mobile robot with two Euler-Bernoulli cooperative manipulators and revolute-prismatic joints was studied in Ref. [24].

As can be understood from the review of existing literature, there is a strong need for an accurate model that can predict the nonlinear behavior of flexible mobile manipulators. In this research, a nonlinear dynamical model of a mobile rigid-elastic Newtonian mechanics system based on the AMM approach is derived, simulated, and compared with the FEM strategy.

Timoshenko's theory is used in the deriving process due to its acceptable accuracy. Another critical issue is the effect of the transverse deformations on the axial behavior. Although the studied arm is supposed to be inextensible, the transverse vibrations of the arm strongly affect its axial behavior, which to the authors' knowledge, has yet to be investigated separately in the general planar motion of a Newtonian mechanics systems including the Timoshenko beam. Therefore, the main innovative aspects of this study can be outlined as follows.

The study develops an efficient, accurate, and reliable dynamic model of flexible mobile manipulators that can be used for behavioral identification and vibration control. Usually, elastic models are necessary in control algorithms to achieve acceptable accuracy in vibration control. For example, the authors recently proposed a control algorithm called optimal rigid-elastic interaction control (OREIC) to control the vibrations of a moving structure carrying a Timoshenko beam[6]. However, these control algorithms usually contain high computational complexity. Thus, it is necessary to ensure that the obtained model of the system is as simple as possible while still being accurate. Therefore, this research presents a much simpler dynamical model than any relevant one available in the literature.

In this research, the correctness and accuracy of the extracted model obtained using the AMM are compared with the FEM in a step-by-step manner, and the results indicate excellent accuracy.

To the best of the authors' knowledge, the effect of the transverse behavior on the axial performance of axially-rigid Timoshenko beams has not been investigated, especially in the general planar motion. Therefore, the effect is studied in detail during the extraction of the dynamic model of the system.

The remainder of this paper is organized as follows. Section 2 provides discussion on the fundamentals of Timoshenko beam modeling as preliminaries. Section 3 addresses the kinematics, kinetics, and reduced-order modeling of the system. Section 4 presents numerical simulations, and discusses and verifies the results. Finally, the study is concluded in Section 5.

2 Preliminaries

2.1 Frequency equation

Consider a straight elastic beam of length ℓ, cross-sectional area $\mathcal{A}$, and cross-sectional area moment of inertia $\mathcal{I}$ with a linear isotropic material of density ϱ, Young's modulus E, and shear modulus G. In addition to the mentioned parameters, depending on the cross-sectional geometry and Poisson's ratio of the material, a physical coefficient named the shear correction factor κ can be calculated for the beam[25]. According to Timoshenko's theory, the governing equations of motion for such a beam under no-loading conditions can be expressed as[26]

$$\frac{\partial}{\partial\xi}\Big(\kappa G\mathcal{A}(\xi)\Big(\frac{\partial w(\xi,t)}{\partial\xi}-\phi(\xi,t)\Big)\Big)-\varrho\mathcal{A}(\xi)\frac{\partial^2 w(\xi,t)}{\partial t^2}=0, \tag{1}$$

$$\frac{\partial}{\partial\xi}\Big(E\mathcal{I}(\xi)\frac{\partial\phi(\xi,t)}{\partial\xi}\Big)+\kappa G\mathcal{A}(\xi)\Big(\frac{\partial w(\xi,t)}{\partial\xi}-\phi(\xi,t)\Big)-\varrho\mathcal{I}(\xi)\frac{\partial^2\phi(\xi,t)}{\partial t^2}=0, \tag{2}$$

where ξ is the spatial variable, t is time, $w(\xi,t):[0,\ell]\times[0,+\infty)\to\mathbb{R}$ is the transverse displacement, and $\phi(\xi,t):[0,\ell]\times[0,+\infty)\to\mathbb{R}$ is the rotation of the beam section due to the bending moment.

For a uniform beam with a homogenous material, Eqs. (1) and (2) can be decoupled as follows:

$$\frac{\partial^4 w(\xi,t)}{\partial\xi^4}-\Big(\frac{\varrho}{E}+\frac{\varrho}{\kappa G}\Big)\frac{\partial^4 w(\xi,t)}{\partial\xi^2\partial t^2}+\frac{\varrho^2}{\kappa GE}\frac{\partial^4 w(\xi,t)}{\partial t^4}+\frac{\varrho\mathcal{A}}{E\mathcal{I}}\frac{\partial^2 w(\xi,t)}{\partial t^2}=0, \tag{3}$$

$$\frac{\partial^4\phi(\xi,t)}{\partial\xi^4}-\Big(\frac{\varrho}{E}+\frac{\varrho}{\kappa G}\Big)\frac{\partial^4\phi(\xi,t)}{\partial\xi^2\partial t^2}+\frac{\varrho^2}{\kappa GE}\frac{\partial^4\phi(\xi,t)}{\partial t^4}+\frac{\varrho\mathcal{A}}{E\mathcal{I}}\frac{\partial^2\phi(\xi,t)}{\partial t^2}=0. \tag{4}$$

In order to solve these equations, it is supposed that there are harmonic solutions as $w(\xi,t)=W(\xi)\mathrm{e}^{\mathrm{i}\omega t}$ and $\phi(\xi,t)=\Phi(\xi)\mathrm{e}^{\mathrm{i}\omega t}$, in which $W(\xi):[0,\ell]\to\mathbb{R}$ and $\Phi(\xi):[0,\ell]\to\mathbb{R}$ are the eigenfunctions of the system satisfying both the governing equations and the boundary conditions, ω is the eigenfrequency or the square root of the eigenvalue, and i is the imaginary unit. Use the following definitions:

$$\mathfrak{r}^2\triangleq\frac{\mathcal{I}}{\mathcal{A}},\quad \zeta\triangleq\frac{E}{\kappa G},\quad \widehat{\omega}^2\triangleq\sqrt{\frac{\varrho\mathcal{A}}{E\mathcal{I}}}\omega. \tag{5}$$

Then, the problem of Eqs. (3) and (4) can be rearranged as boundary value problems,

$$\frac{\mathrm{d}^4W(\xi)}{\mathrm{d}\xi^4}+(1+\zeta)\mathfrak{r}^4\widehat{\omega}^4\frac{\mathrm{d}^2W(\xi)}{\mathrm{d}\xi^2}+(\zeta\mathfrak{r}^4\widehat{\omega}^8-\widehat{\omega}^4)W(\xi)=0, \tag{6}$$

$$\frac{\mathrm{d}^4\Phi(\xi)}{\mathrm{d}\xi^4}+(1+\zeta)\mathfrak{r}^4\widehat{\omega}^4\frac{\mathrm{d}^2\Phi(\xi)}{\mathrm{d}\xi^2}+(\zeta\mathfrak{r}^4\widehat{\omega}^8-\widehat{\omega}^4)\Phi(\xi)=0. \tag{7}$$

The characteristic equations of Eqs. (6) and (7) contain four roots γ_1, γ_2, γ_3, and γ_4 as follows:

$$\begin{cases}\gamma_1=-\widehat{\omega}\sqrt{-\Big(\frac{1+\zeta}{2}\Big)\mathfrak{r}^2\widehat{\omega}^2-\sqrt{\Big(\frac{1-\zeta}{2}\Big)^2\mathfrak{r}^4\widehat{\omega}^4+1}},\\ \gamma_2=\widehat{\omega}\sqrt{-\Big(\frac{1+\zeta}{2}\Big)\mathfrak{r}^2\widehat{\omega}^2-\sqrt{\Big(\frac{1-\zeta}{2}\Big)^2\mathfrak{r}^4\widehat{\omega}^4+1}},\\ \gamma_3=-\widehat{\omega}\sqrt{-\Big(\frac{1+\zeta}{2}\Big)\mathfrak{r}^2\widehat{\omega}^2+\sqrt{\Big(\frac{1-\zeta}{2}\Big)^2\mathfrak{r}^4\widehat{\omega}^4+1}},\\ \gamma_4=\widehat{\omega}\sqrt{-\Big(\frac{1+\zeta}{2}\Big)\mathfrak{r}^2\widehat{\omega}^2+\sqrt{\Big(\frac{1-\zeta}{2}\Big)^2\mathfrak{r}^4\widehat{\omega}^4+1}}.\end{cases} \tag{8}$$

Assume $\widehat{\omega}\neq 0$. It is obvious that γ_1 and γ_2 are the imaginary conjugate roots such that using the definition

$$\alpha\triangleq\widehat{\omega}\sqrt{\Big(\frac{1+\zeta}{2}\Big)\mathfrak{r}^2\widehat{\omega}^2+\sqrt{\Big(\frac{1-\zeta}{2}\Big)^2\mathfrak{r}^4\widehat{\omega}^4+1}}, \tag{9}$$

they can be described as $\gamma_1=-\mathrm{i}\alpha$ and $\gamma_2=+\mathrm{i}\alpha$. However, in the case of γ_3 and γ_4, two different situations are possible. If $\widehat{\omega}<\frac{1}{\mathfrak{r}\sqrt[4]{\zeta}}$, or $\omega<\sqrt{\frac{\kappa G\mathcal{A}}{\varrho\mathcal{I}}}$, γ_3 and γ_4 become two real symmetric roots such that using the definition

$$\beta\triangleq\widehat{\omega}\sqrt{-\Big(\frac{1+\zeta}{2}\Big)\mathfrak{r}^2\widehat{\omega}^2+\sqrt{\Big(\frac{1-\zeta}{2}\Big)^2\mathfrak{r}^4\widehat{\omega}^4+1}}, \tag{10}$$

they can be expressed as $\gamma_3=-\beta$ and $\gamma_4=+\beta$. In the case of $\omega>\sqrt{\frac{\kappa G\mathcal{A}}{\varrho\mathcal{I}}}$, they become two imaginary conjugate roots such that using the definition

$$\beta'\triangleq\widehat{\omega}\sqrt{\Big(\frac{1+\zeta}{2}\Big)\mathfrak{r}^2\widehat{\omega}^2-\sqrt{\Big(\frac{1-\zeta}{2}\Big)^2\mathfrak{r}^4\widehat{\omega}^4+1}}, \tag{11}$$

they can be presented as $\gamma_3=-\mathrm{i}\beta'$ and $\gamma_4=+\mathrm{i}\beta'$. The cut-off frequency $\omega_0=\sqrt{\frac{\kappa G\mathcal{A}}{\varrho\mathcal{I}}}$ is called the critical frequency[27], and higher eigenfrequencies of the system are known as the

second spectrum of frequencies[19]. Therefore, for the case of $\omega < \sqrt{\frac{\kappa G\mathcal{A}}{\varrho\mathcal{I}}}$, the eigenfunctions are combinations of harmonic and hyperbolic functions such as

$$\begin{cases} W(\xi) = \mathcal{C}_1 \sin(\alpha\xi) + \mathcal{C}_2 \cos(\alpha\xi) + \mathcal{C}_3 \sinh(\beta\xi) + \mathcal{C}_4 \cosh(\beta\xi), \\ \Phi(\xi) = \mathcal{D}_1 \sin(\alpha\xi) + \mathcal{D}_2 \cos(\alpha\xi) + \mathcal{D}_3 \sinh(\beta\xi) + \mathcal{D}_4 \cosh(\beta\xi). \end{cases} \tag{12}$$

In the second spectrum, the eigenfunctions of the system are full-harmonic as follows[27]:

$$\begin{cases} W'(\xi) = \mathcal{C}'_1 \sin(\alpha\xi) + \mathcal{C}'_2 \cos(\alpha\xi) + \mathcal{C}'_3 \sin(\beta'\xi) + \mathcal{C}'_4 \cos(\beta'\xi), \\ \Phi'(\xi) = \mathcal{D}'_1 \sin(\alpha\xi) + \mathcal{D}'_2 \cos(\alpha\xi) + \mathcal{D}'_3 \sin(\beta'\xi) + \mathcal{D}'_4 \cos(\beta'\xi). \end{cases} \tag{13}$$

Considering Eqs. (1) and (2), the definitions provided as follows:

$$\lambda_1 \triangleq \frac{\zeta\mathfrak{r}^2\widehat{\omega}^4 - \alpha^2}{\alpha}, \quad \lambda_2 \triangleq \frac{\zeta\mathfrak{r}^2\widehat{\omega}^4 + \beta^2}{\beta}, \quad \lambda'_1 \triangleq \frac{\zeta\mathfrak{r}^2\widehat{\omega}^4 - \alpha^2}{\alpha}, \quad \lambda'_2 \triangleq \frac{\zeta\mathfrak{r}^2\widehat{\omega}^4 - \beta'^2}{\beta'}, \tag{14}$$

$$\begin{cases} \mathfrak{A}_{11} = -\frac{m_0}{\varrho\mathcal{A}}\zeta\mathfrak{r}^2\widehat{\omega}^4 \sin(\alpha\ell) + (\alpha + \lambda_1)\cos(\alpha\ell) - \frac{m_0}{\varrho\mathcal{A}}\frac{\lambda_1}{\lambda_2}\zeta\mathfrak{r}^2\widehat{\omega}^4 \sinh(\beta\ell) \\ \qquad + \lambda_1\Big(\frac{\beta}{\lambda_2} - 1\Big)\cosh(\beta\ell), \\ \mathfrak{A}_{12} = -\frac{m_0}{\varrho\mathcal{A}}\zeta\mathfrak{r}^2\widehat{\omega}^4 \cos(\alpha\ell) - (\alpha + \lambda_1)\sin(\alpha\ell) + \frac{m_0}{\varrho\mathcal{A}}\zeta\mathfrak{r}^2\widehat{\omega}^4 \cosh(\beta\ell) - (\beta - \lambda_2)\sinh(\beta\ell), \\ \mathfrak{A}_{21} = \lambda_1\alpha \sin(\alpha\ell) + \frac{\mathcal{J}_0}{\varrho\mathcal{A}}\lambda_1\widehat{\omega}^4 \cos(\alpha\ell) + \lambda_1\beta \sinh(\beta\ell) - \frac{\mathcal{J}_0}{\varrho\mathcal{A}}\lambda_1\widehat{\omega}^4 \cosh(\beta\ell), \\ \mathfrak{A}_{22} = \lambda_1\alpha \cos(\alpha\ell) - \frac{\mathcal{J}_0}{\varrho\mathcal{A}}\lambda_1\widehat{\omega}^4 \sin(\alpha\ell) - \lambda_2\beta \cosh(\beta\ell) + \frac{\mathcal{J}_0}{\varrho\mathcal{A}}\lambda_2\widehat{\omega}^4 \sinh(\beta\ell), \\ \mathfrak{A}'_{11} = -\frac{m_0}{\varrho\mathcal{A}}\zeta\mathfrak{r}^2\widehat{\omega}^4 \sin(\alpha\ell) + (\alpha + \lambda'_1)\cos(\alpha\ell) + \frac{m_0}{\varrho\mathcal{A}}\frac{\lambda'_1}{\lambda'_2}\zeta\mathfrak{r}^2\widehat{\omega}^4 \sin(\beta'\ell) \\ \qquad - \lambda'_1\Big(\frac{\beta'}{\lambda'_2} - 1\Big)\cos(\beta'\ell), \\ \mathfrak{A}'_{12} = -\frac{m_0}{\varrho\mathcal{A}}\zeta\mathfrak{r}^2\widehat{\omega}^4 \cos(\alpha\ell) - (\alpha + \lambda'_1)\sin(\alpha\ell) + \frac{m_0}{\varrho\mathcal{A}}\zeta\mathfrak{r}^2\widehat{\omega}^4 \cos(\beta'\ell) + (\beta' + \lambda'_2)\sin(\beta'\ell), \\ \mathfrak{A}'_{21} = \lambda'_1\alpha \sin(\alpha\ell) + \frac{\mathcal{J}_0}{\varrho\mathcal{A}}\lambda'_1\widehat{\omega}^4 \cos(\alpha\ell) - \lambda'_1\beta' \sin(\beta'\ell) - \frac{\mathcal{J}_0}{\varrho\mathcal{A}}\lambda'_1\widehat{\omega}^4 \cos(\beta'\ell), \\ \mathfrak{A}'_{22} = \lambda'_1\alpha \cos(\alpha\ell) - \frac{\mathcal{J}_0}{\varrho\mathcal{A}}\lambda'_1\widehat{\omega}^4 \sin(\alpha\ell) - \lambda'_2\beta' \cos(\beta'\ell) + \frac{\mathcal{J}_0}{\varrho\mathcal{A}}\lambda'_2\widehat{\omega}^4 \sin(\beta'\ell), \end{cases} \tag{15}$$

the clamped boundary condition at $\xi = 0$, and a rigid tip mass m_0 with the moment of inertia $\mathcal{J}_0$ at $\xi = \ell$, the frequency equations of the system can be expressed as follows:

$$\mathfrak{A}_{11}\mathfrak{A}_{22} - \mathfrak{A}_{12}\mathfrak{A}_{21} = 0, \tag{16}$$

$$\mathfrak{A}'_{11}\mathfrak{A}'_{22} - \mathfrak{A}'_{12}\mathfrak{A}'_{21} = 0. \tag{17}$$

After solving the frequency equations, the nth natural frequency of the system can be obtained as ω_n, and using the subscript n for other related parameters, the eigenfunctions of the first and second spectra of the system can be expressed as

$$\begin{cases} W_n(\xi) = \mathcal{C}_n\Big(\sin(\alpha_n\xi) - \frac{\mathfrak{A}_{21_n}}{\mathfrak{A}_{22_n}}\cos(\alpha_n\xi) + \frac{\lambda_{1_n}}{\lambda_{2_n}}\sinh(\beta_n\xi) + \frac{\mathfrak{A}_{21_n}}{\mathfrak{A}_{22_n}}\cosh(\beta_n\xi)\Big), \\ \Phi_n(\xi) = \mathcal{C}_n\Big(-\frac{\mathfrak{A}_{21_n}}{\mathfrak{A}_{22_n}}\lambda_{1_n}\sin(\alpha_n\xi) - \lambda_{1_n}\cos(\alpha_n\xi) + \frac{\mathfrak{A}_{21_n}}{\mathfrak{A}_{22_n}}\lambda_{2_n}\sinh(\beta_n\xi) \\ \qquad + \lambda_{1_n}\cosh(\beta_n\xi)\Big), \end{cases} \tag{18}$$

where $n = 1, 2, \cdots, \mathfrak{N}$.

$$\begin{cases} W'_n(\xi) = \mathcal{C}'_n\Big(\sin(\alpha_n\xi) - \dfrac{\mathfrak{A}'_{21_n}}{\mathfrak{A}'_{22_n}}\cos(\alpha_n\xi) - \dfrac{\lambda'_{1_n}}{\lambda'_{2_n}}\sin(\beta'_n\xi) + \dfrac{\mathfrak{A}'_{21_n}}{\mathfrak{A}'_{22_n}}\cos(\beta'_n\xi)\Big), \\ \Phi'_n(\xi) = \mathcal{C}'_n\Big(-\dfrac{\mathfrak{A}'_{21_n}}{\mathfrak{A}'_{22_n}}\lambda'_{1_n}\sin(\alpha_n\xi) - \lambda'_{1_n}\cos(\alpha_n\xi) + \dfrac{\mathfrak{A}'_{21_n}}{\mathfrak{A}'_{22_n}}\lambda'_{2_n}\sin(\beta'_n\xi) \\ \qquad\qquad + \lambda'_{1_n}\cos(\beta'_n\xi)\Big), \end{cases} \tag{19}$$

where $n = \mathfrak{N}+1, \mathfrak{N}+2, \cdots$. $\mathfrak{N}$ is the number of elements in the set of the first spectrum of frequencies, and $\omega_{\mathfrak{N}}$ denotes the greatest natural frequency in this set.

2.2 Orthogonality of eigenfunctions

Consider a Timoshenko beam with the arbitrary axial mass and inertia distributions of $\mathcal{M}(\xi)$ and $\mathcal{J}(\xi)$, respectively. Timoshenko's model for such a beam under no-loading conditions can be expressed in a matrix form as follows:

$$\begin{bmatrix} \dfrac{\partial}{\partial\xi}\Big(\kappa G\mathcal{A}(\xi)\dfrac{\partial(\cdot)}{\partial\xi}\Big) & \dfrac{\partial}{\partial\xi}(\kappa G\mathcal{A}(\xi)(\cdot)) \\ \kappa G\mathcal{A}(\xi)\dfrac{\partial(\cdot)}{\partial\xi} & \dfrac{\partial}{\partial\xi}\Big(E\mathcal{I}(\xi)\dfrac{\partial(\cdot)}{\partial\xi}\Big) - \kappa G\mathcal{A}(\xi)(\cdot) \end{bmatrix} \begin{bmatrix} w(\xi,t) \\ \phi(\xi,t) \end{bmatrix} \\ - \begin{bmatrix} \mathcal{M}(\xi) & 0 \\ 0 & \mathcal{J}(\xi) \end{bmatrix} \begin{bmatrix} \dfrac{\partial^2 w(\xi,t)}{\partial t^2} \\ \dfrac{\partial^2\phi(\xi,t)}{\partial t^2} \end{bmatrix} = \mathbf{0}. \tag{20}$$

It is important to note that in Eq. (20), upon multiplying the first square matrix with the subsequent vector, $w(\xi,t)$ and $\phi(\xi,t)$ are replaced with the symbol $(\cdot)$.

Remark 1 The arbitrary distributions of axial mass and inertia addressed in Eq. (20) could involve local concentrated mass and inertia. As an example, for a uniform homogeneous beam clamped at $\xi = 0$, with an attached rigid body of mass m_0 and inertia $\mathcal{J}_0$ at $\xi = \ell$, the mass and inertia distributions can be expressed as $\mathcal{M}(\xi) = \varrho\mathcal{A} + m_0\delta(\xi-\ell)$ and $\mathcal{J} = \varrho\mathcal{I} + \mathcal{J}_0\delta(\xi-\ell)$, respectively, in which $\delta(\xi-\ell)$ refers to Dirac's delta function at the point $\xi = \ell$.

Considering Eq. (20) and using separation of variables strategy, for any pair of distinct vectors of eigenfunctions $\begin{bmatrix} W_m(\xi) & \Phi_m(\xi) \end{bmatrix}^{\mathrm{T}}$ and $\begin{bmatrix} W_n(\xi) & \Phi_n(\xi) \end{bmatrix}^{\mathrm{T}}$, we can obtain

$$\int_0^\ell \begin{bmatrix} W_m(\xi) & \Phi_m(\xi) \end{bmatrix} \begin{bmatrix} \mathcal{M}(\xi) & 0 \\ 0 & \mathcal{J}(\xi) \end{bmatrix} \begin{bmatrix} W_n(\xi) \\ \Phi_n(\xi) \end{bmatrix} \mathrm{d}\xi = 0. \tag{21}$$

Equation (21) represents the first form of eigenfunction orthogonality of the Timoshenko beam. The second form for $m \neq n$ can be obtained as follows:

$$\int_0^\ell \begin{bmatrix} W_m(\xi) & \Phi_m(\xi) \end{bmatrix} \begin{bmatrix} \dfrac{\mathrm{d}}{\mathrm{d}\xi}\Big(\kappa G\mathcal{A}(\xi)\dfrac{\mathrm{d}(\cdot)}{\mathrm{d}\xi}\Big) & -\dfrac{\mathrm{d}}{\mathrm{d}\xi}\Big(\kappa G\mathcal{A}(\xi)(\cdot)\Big) \\ \kappa G\mathcal{A}(\xi)\dfrac{\mathrm{d}(\cdot)}{\mathrm{d}\xi} & \dfrac{\mathrm{d}}{\mathrm{d}\xi}\Big(E\mathcal{I}(\xi)\dfrac{\mathrm{d}(\cdot)}{\mathrm{d}\xi} - \kappa G\mathcal{A}(\xi)(\cdot)\Big) \end{bmatrix} \\ \times \begin{bmatrix} W_n(\xi) \\ \Phi_n(\xi) \end{bmatrix} \mathrm{d}\xi = 0. \tag{22}$$

Remark 2 If the two coefficients $\mathcal{C}_n$ and $\mathcal{C}'_n$ in Eqs. (18) and (19) are chosen such that the relationship

$$\int_0^\ell \begin{bmatrix} W_n(\xi) & \Phi_n(\xi) \end{bmatrix} \begin{bmatrix} \mathcal{M}(\xi) & 0 \\ 0 & \mathcal{J}(\xi) \end{bmatrix} \begin{bmatrix} W_n(\xi) \\ \Phi_n(\xi) \end{bmatrix} \mathrm{d}\xi = 1 \tag{23}$$

holds for any natural mode of the system, then the sequence of eigenfunction vectors $[W_n(\xi)\ \Phi_n(\xi)]^{\mathrm{T}}$ $(n = 1, 2, \cdots)$ will be an orthonormal set of eigenfunctions. In such a situation, for $n = m$, we can obtain

$$\int_0^\ell [W_n(\xi) \quad \Phi_n(\xi)] \begin{bmatrix} \frac{\mathrm{d}}{\mathrm{d}\xi}\left(\kappa(\xi)G(\xi)\mathcal{A}(\xi)\frac{\mathrm{d}(\cdot)}{\mathrm{d}\xi}\right) & -\frac{\mathrm{d}}{\mathrm{d}\xi}(\kappa(\xi)G(\xi)\mathcal{A}(\xi)(\cdot)) \\ \kappa(\xi)G(\xi)\mathcal{A}(\xi)\frac{\mathrm{d}(\cdot)}{\mathrm{d}\xi} & \frac{\mathrm{d}}{\mathrm{d}\xi}(E(\xi)\mathcal{I}(\xi)\frac{\mathrm{d}(\cdot)}{\mathrm{d}\xi} - \kappa(\xi)G(\xi)\mathcal{A}(\xi)(\cdot)) \end{bmatrix} \times \begin{bmatrix} W_n(\xi) \\ \Phi_n(\xi) \end{bmatrix} \mathrm{d}\xi = -\omega_n^2. \tag{24}$$

3 Dynamical modeling

3.1 Configuration and kinematics

Figure 1 illustrates a schematic configuration of a planar mobile single-link flexible manipulator positioned on a horizontal plane. The system consists of a rigid carrier of mass m_{c}, restricted to translate in the plane without rotation under the action of horizontal and vertical applying forces $F_x(t)$ and $F_y(t)$. A rotary motor of mass m_{m} and shaft moment of inertia $\mathcal{J}_{\mathrm{m}}$ is also mounted on the rigid carrier. A torque $\tau_\theta(t)$ is exerted on the output shaft of the motor, which makes it rotate along with its clamped flexible Timoshenko arm. In order to manipulate objects, an approximately dimensionless rigid end-effector of mass m_{e} and moment of inertia $\mathcal{J}_{\mathrm{e}}$ is attached to the arm as a tip mass/inertia.

Two coordinate systems are utilized to describe the rigid body motion and flexible behavior, i.e., an inertial reference frame "xOy" and a moving-rotating reference frame "IO'II". The moving-rotating reference frame, originating at the shaft center, follows all types of shaft motion. It is evident that the beam section at $\xi = 0$ is always perpendicular to the I-axis of the moving-rotating frame, and the transverse deformations of the beam are described with respect to this axis. Suppose that the horizontal and vertical components of the carrier position are expressed as $x_{\mathrm{c}}(t)$ and $y_{\mathrm{c}}(t)$, respectively. In that case, the acceleration of each point on the beam's neutral axis can be obtained as follows:

$$\frac{\partial^2 r(\xi, t)}{\partial t^2} = \mathfrak{a}_{\mathrm{I}}(\xi, t)e_{\mathrm{I}} + \mathfrak{a}_{\mathrm{II}}(\xi, t)e_{\mathrm{II}}, \tag{25}$$

where e_{I} and e_{II} refer to the unit vectors in the I-, and II-directions, respectively, and $\mathfrak{a}_{\mathrm{I}}$ and

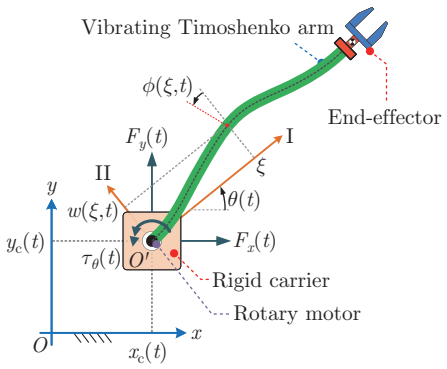

Fig. 1 Schematic configuration of a planar mobile single-link flexible manipulator (color online)

$\mathfrak{a}_{\mathrm{II}}$ can be calculated by

$$\mathfrak{a}_{\mathrm{I}}(\xi,t) = -w(\xi,t)\ddot{\theta}(t) - 2\dot{\theta}(t)\frac{\partial w(\xi,t)}{\partial t} - \xi\dot{\theta}^2(t) + \ddot{x}_{\mathrm{c}}(t)\cos(\theta(t)) + \ddot{y}_{\mathrm{c}}(t)\sin(\theta(t)), \tag{26}$$

$$\mathfrak{a}_{\mathrm{II}}(\xi,t) = \frac{\partial^2 w(\xi,t)}{\partial t^2} + \xi\ddot{\theta}(t) - w(\xi,t)\dot{\theta}^2(t) - \ddot{x}_{\mathrm{c}}(t)\sin(\theta(t)) + \ddot{y}_{\mathrm{c}}(t)\cos(\theta(t)). \tag{27}$$

3.2 Kinetics of flexible arm

A differential element of the Timoshenko beam of length $\mathrm{d}\xi$, axial mass distribution $\mathcal{M}(\xi)$, and axial moment of inertia distribution $\mathcal{J}(\xi)$ under the action of axial force $P(\xi,t)$, shear force $V(\xi,t)$, and bending moment $M(\xi,t)$ is shown in Fig. 2. Using Newton's second law and the kinematics of the neutral axis represented in Eq. (27), the governing equation of motion for the element in the transverse direction can be presented as[28]

$$\frac{\partial}{\partial\xi}\Big(\kappa(\xi)G(\xi)\mathcal{A}(\xi)\Big(\frac{\partial w(\xi,t)}{\partial\xi} - \phi(\xi,t)\Big)\Big) - \mathcal{M}(\xi)\mathfrak{a}_{\mathrm{II}}(\xi,t) = 0. \tag{28}$$

For the rotation of the beam elements, using the Newton-Euler laws, we can obtain[28]

$$\frac{\partial}{\partial\xi}\Big(E\mathcal{I}(\xi)\frac{\partial\phi(\xi,t)}{\partial\xi}\Big) + \kappa G\mathcal{A}(\xi)\Big(\frac{\partial w(\xi,t)}{\partial\xi} - \phi(\xi,t)\Big) - \mathcal{J}(\xi)\Big(\ddot{\theta}(t) + \frac{\partial^2\phi(\xi,t)}{\partial t^2}\Big) = 0. \tag{29}$$

Finally, the governing equation for the axial direction can be obtained in an exact differential form and solved as follows:

$$P(\xi,t) = P(0,t) + \int_0^{\xi}\mathcal{M}(\xi)\mathfrak{a}_{\mathrm{I}}(\xi,t)\mathrm{d}\xi. \tag{30}$$

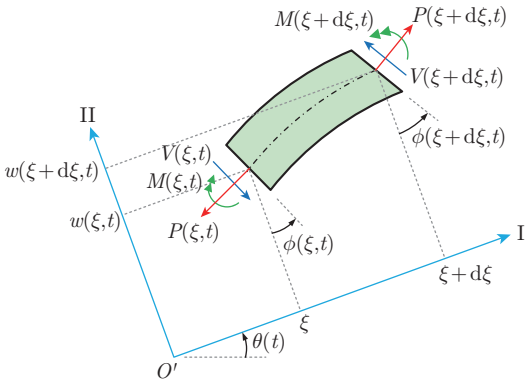

Fig. 2 A differential element of the flexible Timoshenko arm in the moving-rotating reference frame (color online)

3.3 Kinetics of rigid components

The free body diagrams (FBDs) of the carrier, motor, and arm are illustrated in Fig. 3. According to Fig. 3, the governing equations of the rigid carrier and motor can be presented as

$$(m_{\mathrm{c}} + m_{\mathrm{m}})\ddot{x}_{\mathrm{c}}(t) = P(0,t)\cos(\theta(t)) - V(0,t)\sin(\theta(t)) + F_x(t), \tag{31}$$

$$(m_{\mathrm{c}} + m_{\mathrm{m}})\ddot{y}_{\mathrm{c}}(t) = P(0,t)\sin(\theta(t)) + V(0,t)\sin(\theta(t)) + F_y(t), \tag{32}$$

$$\mathcal{J}_{\mathrm{m}}\ddot{\theta}(t) = M(0,t) + \tau_\theta(t), \tag{33}$$

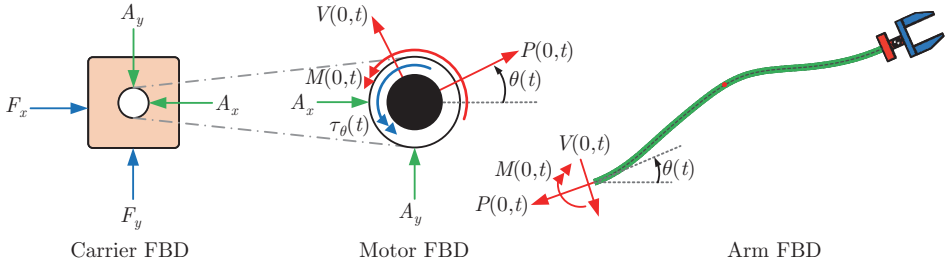

Fig. 3 FBDs of the rigid carrier, rotary motor, and flexible arm (color online)

where $V(0,t)$ and $M(0,t)$ can be calculated according to Timoshenko's theory[28]. Additionally, taking into account Eq. (30) and utilizing the boundary condition $P(\ell,t)=0$, we can derive

$$P(0,t)=-\int_0^\ell \mathcal{M}(\xi)\mathfrak{a}_{\mathrm{I}}(\xi,t)\mathrm{d}\xi. \tag{34}$$

Remark 4 In this study, the transverse and bending deformations of the beam are taken into account, while the axial deformation is neglected. Therefore, it can be concluded that according to the axial rigidity of the beam, the assumption of rigid body dynamics holds true in the axial direction. This means that "the net axial force acting on the arm in the axial direction equals its mass times the axial acceleration of its mass center." This expression can be formulated as

$$\widetilde{P}(0,t)=-\Big(\int_0^\ell \mathcal{M}(\xi)\mathrm{d}\xi\Big)\mathfrak{a}_{\mathrm{I}}(\chi,t), \tag{35}$$

in which $\widetilde{P}(0,t)$ refers to the axial force acting on the beam with the assumption of rigid body dynamics, and χ is the axial component of the beam mass center in the moving-rotating reference frame. However, it is crucial to note that while the beam is assumed to be rigid in the axial direction, its axial acceleration does not contain only axial effects but also the effects of transverse deformation. The improper use of $\widetilde{P}(0,t)$ instead of $P(0,t)$ can result in a significant error in predicting the system's behavior, which will be further discussed in the simulations.

3.4 Reduced-order modeling

In this study, the AMM approach is used to describe the vibrational behavior of the flexible arm. In this regard, considering the eigenfunctions $W_n(\xi)$ and $\Phi_n(\xi)$ $(n=1,2,\cdots)$, it is assumed that the elastic behavior of the beam is expandable as

$$w(\xi,t)=\sum_{n=1}^{\infty}W_n(\xi)q_n(t),\quad \phi(\xi,t)=\sum_{n=1}^{\infty}\Phi_n(\xi)q_n(t), \tag{36}$$

in which $q_n(t)$ is a time-dependent generalized coordinate.

According to the selected coordinates and degrees of freedom considered for the system, it is clear that the clamped boundary condition rules at the point $\xi=0$. If the mass and mass moment of inertia of the end-effector are considered in the mass and inertia distribution as $\mathcal{M}(\xi)=\varrho\mathcal{A}(\xi)+m_{\mathrm{e}}\delta(\xi-\ell)$ and $\mathcal{J}(\xi)=\varrho\mathcal{I}(\xi)+\mathcal{J}_{\mathrm{e}}\delta(\xi-\ell)$, respectively, it can be concluded that the arm is free at $\xi=\ell$.

Substituting Eq. (36) into Eq. (20) and applying the AMM approach with the consideration of the orthogonality property, we can evaluate the flexible behavior of the system. This, along with Eqs. (31)–(33), constitutes the assumed mode model for the planar mobile single-link flexible Timoshenko manipulator.

4 Simulation results, discussion, and verification

In this section, the numerical simulation results will be presented, and the performance and accuracy of the proposed model will be examined. Commercial software (Student version of ANSYS 2023R1 Mechanical APDL, Ansys Inc.) is utilized to check the FEM-based validity of the model. In this regard, the arm can be modeled using the BEAM188 3-D 2-Node Timoshenko's theory-based beam element, and the concentrated mass/inertia can be modeled using the MASS21 structural mass element.

In the current simulations, it is assumed that the flexible arm has a uniform rectangular cross section and is made of a homogeneous material. In this case, considering Poisson's ratio of the material ν, the shear correction factor κ for such a section can be calculated as follows[25]:

$$\kappa = \frac{10(1+\nu)}{12+11\nu}. \tag{37}$$

The physical, mechanical, and geometrical specifications of the system components, including the flexible arm, carrier, motor, and end-effector, are listed in Table 1.

Table 1 Physical, mechanical, and geometrical specifications of the mobile single-link flexible manipulator

Symbol	Description	Value	Unit
ℓ	Arm length	2	m
$\mathcal{A}$	Cross-sectional area	$(20\times10^{-3})\times(20\times10^{-3})$	m^2
$\mathcal{I}$	Cross-sectional area moment of inertia	$\frac{1}{12}\times(20\times10^{-3})\times(20\times10^{-3})^3$	m^4
ϱ	Mass density of beam material	2 710	$\mathrm{kg/m}^2$
E	Young's modulus of beam material	70.5×10^9	Pa
G	Shear modulus of beam material	27×10^9	Pa
ν	Poisson's ratio of beam material	0.31	–
κ	Shear correction factor	0.85	–
m_c	Carrier mass	5	kg
m_m	Motor mass	5	kg
$\mathcal{J}_\mathrm{m}$	Mass moment of inertia of motor shaft	2	$\mathrm{kg}\cdot\mathrm{m}^2$
m_e	Mass of end-effector	2	kg
$\mathcal{J}_\mathrm{e}$	Mass moment of inertia of end-effector	0.5	$\mathrm{kg}\cdot\mathrm{m}^2$

4.1 Modal analysis

The natural frequencies of an arm clamped at one end with an attached mass/inertia at the other are calculated analytically regarding the specifications listed in Table 1. To evaluate and validate the resulting values, the natural frequencies of the mentioned system are also calculated using the FEM, and the results of both methods are listed in Table 2 for the first five natural frequencies. Table 2 indicates that there is a small error percentage for the calculated natural frequencies.

Table 2 Comparison of the first five natural frequencies obtained from the analytical method according to Eq. (16) and the FEM analysis in the commercial software ANSYS 2023R1 Mechanical APDL

Mode number	Analytical method/Hz	FEM analysis/Hz	Error/%
1	1.786 9	1.787 5	0.04
2	9.073 8	9.074 0	0.00
3	29.810 8	29.810 7	0.00
4	74.990 2	74.989 3	0.00
5	143.887 2	143.884 1	0.00

In the following, the orthonormal eigenfunctions are obtained using Eqs. (18) and compared with the results using the FEM. The comparison of these results for the first six mode shapes

is shown in Fig. 4 for transverse mode shapes and Fig. 5 for rotational mode shapes.

Remark 5 According to the relationship $\omega_0 = \sqrt{\frac{\kappa G \mathcal{A}}{\varrho \mathcal{I}}}$, a cut-off frequency value equal to 80 217 is obtained on the scale of Hz, which is considered very large concerning the first five

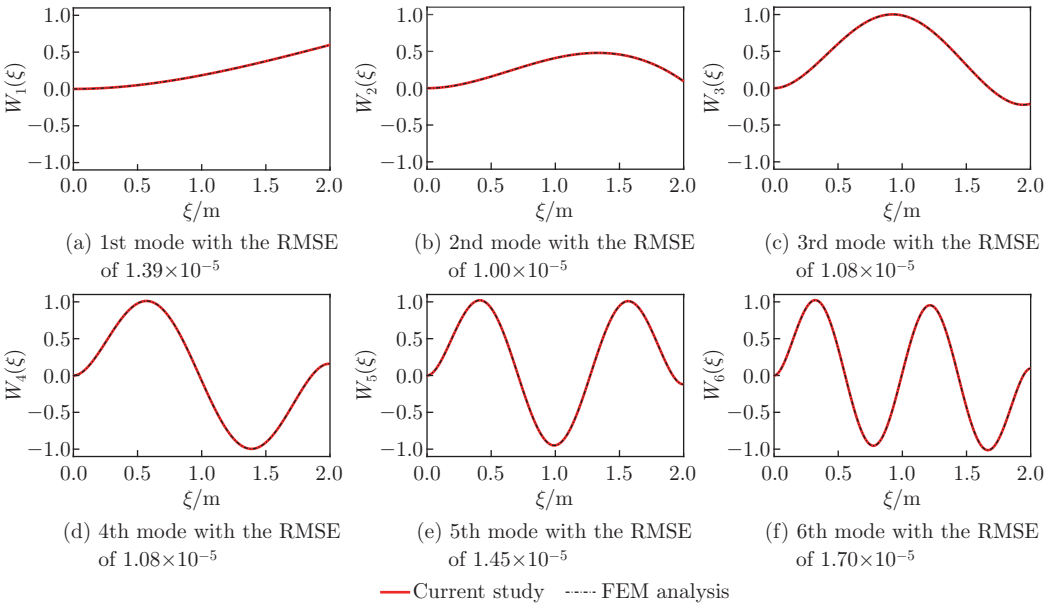

(a) 1st mode with the RMSE of 1.39×10^{-5}
(b) 2nd mode with the RMSE of 1.00×10^{-5}
(c) 3rd mode with the RMSE of 1.08×10^{-5}
(d) 4th mode with the RMSE of 1.08×10^{-5}
(e) 5th mode with the RMSE of 1.45×10^{-5}
(f) 6th mode with the RMSE of 1.70×10^{-5}

Fig. 4 Orthogonal transverse eigenfunctions of the uniform homogenous Timoshenko arm clamped at one end with an attached mass/inertia at the other, where the root mean square error (RMSE) is calculated for each eigenfunction to quantify the error between the FEM and the proposed method across the beam length (color online)

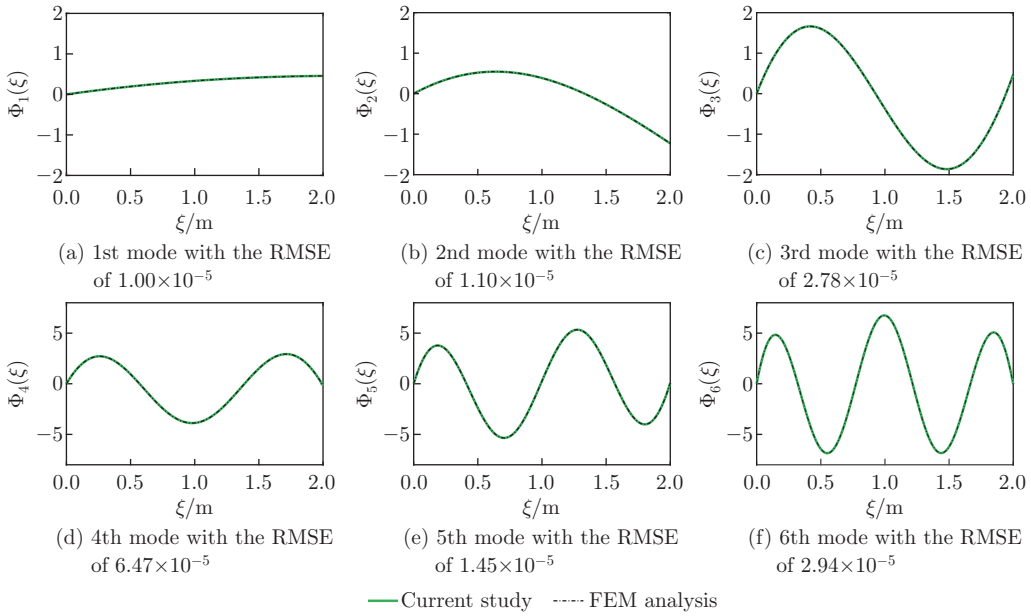

(a) 1st mode with the RMSE of 1.00×10^{-5}
(b) 2nd mode with the RMSE of 1.10×10^{-5}
(c) 3rd mode with the RMSE of 2.78×10^{-5}
(d) 4th mode with the RMSE of 6.47×10^{-5}
(e) 5th mode with the RMSE of 1.45×10^{-5}
(f) 6th mode with the RMSE of 2.94×10^{-5}

Fig. 5 Orthogonal rotational eigenfunctions of the uniform homogenous Timoshenko arm clamped at one end with an attached mass/inertia at the other (color online)

natural frequencies. Considering both analytical (such as the mode superposition technique) and approximate methods (such as the AMM), only a limited number of the first eigenfunctions of the system are used. Therefore, the calculation of the eigenfunctions of the second spectrum is not necessary.

4.2 Transient analysis

The transient analysis of the system under the effect of external loads is carried out for further evaluation. It is assumed that the system is initially at rest, and its other initial conditions are in accord with the data in Table 3. Also, external loadings are considered in a harmonic form, and their patterns are presented in Table 4. For comparison, an FEM analysis with a mesh size of 1 cm for the elastic arm has been carried out using the commercial software ANSYS 2023R1 Mechanical APDL.

Table 3 Position-related initial conditions of the system considered in the transient analysis, where the system is assumed to be at rest at the beginning of the motion

Initial condition	Description	Value	Unit
$x_c(0)$	Horizontal position of the carrier at the beginning	0	m
$y_c(0)$	Vertical position of the carrier at the beginning	0	m
$\theta(0)$	Angular position of the shaft at the beginning	45	deg
$w(\xi, 0)$	Initial transverse deflection of the arm	0	m
$\phi(\xi, 0)$	Initial rotation of the beam sections due to bending	0	rad

Table 4 Specification of the external harmonic loadings applied to the system

External excitation	Amplitude	Frequency/Hz	Pattern	Unit
$F_x(t)$	5	2	$5\sin(4\pi t)$	N
$F_y(t)$	5	3	$5\sin(6\pi t)$	N
$\tau_\theta(t)$	5	4	$5\sin(8\pi t)$	N · m

The time histories of the horizontal, vertical, and angular positions of different system points are shown in Figs. 6–8, respectively. In each figure, the segment (a) belongs to the response of the system at $\xi = 0$, which represents the location of the carrier, the motor, and the initial section of the elastic arm. The segments (b), (c), and (d) are related to $\xi = \frac{\ell}{4}$, $\xi = \frac{\ell}{2}$, and $\xi = \frac{3\ell}{4}$, respectively, and the segment (e) shows the behavior of the system at $\xi = \ell$, which corresponds to the end section of the arm and the end-effector. By examining Figs. 6–8 and comparing the results with the FEM, one can understand the high accuracy of the extracted model of the system.

In addition to the general in-plane motion, the elastic deformations of the system, including the transverse deflection of Timoshenko's arm and the rotation of its sections due to bending, are studied. The results are presented in Figs. 9 and 10, respectively. In each figure, the segments (a), (b), and (c) belong to $\xi = \frac{\ell}{4}$, $\xi = \frac{\ell}{2}$, and $\frac{3\ell}{4}$, respectively, and the segment (d) belongs to the end section $\xi = \ell$, which represents the location of the end-effector. Figures 9 and 10 show that the proposed model is capable of highly accurate predictions, not only for the general rigid body motion of the system but also for its elastic behavior. Additionally, as illustrated in Fig. 9, the elastic arm undergoes a relatively large transverse deformation compared with its length, such that according to Fig. 9(d), the deflection amount in $\xi = \ell$ reaches about approximately 80 mm. However, according to Fig. 10, the rotation of the sections remains less than 4.5 degrees. Despite the large lateral deformations, the linearity assumption for the elastic behavior of the arm is always valid.

The error analyses for the horizontal, vertical, and angular positions of different points are shown in Figs. 11(a), 11(b), and 11(c), respectively. According to these figures, it can be seen that the proposed model shows a comparatively small error compared with the FEM.

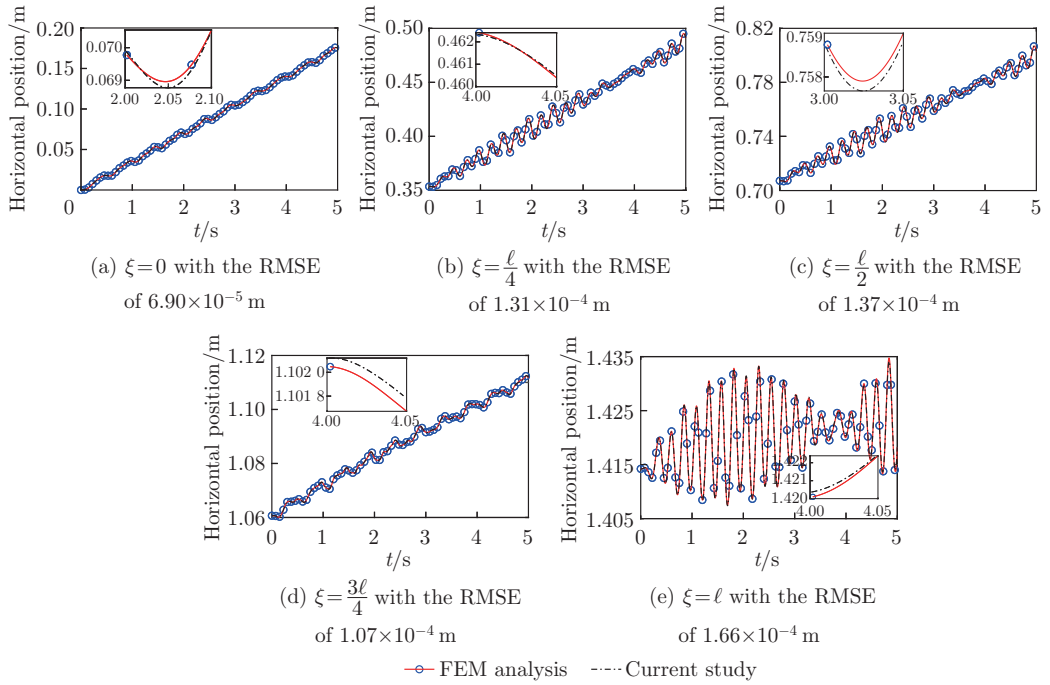

Fig. 6 Time histories of the horizontal position of different points of the system (color online)

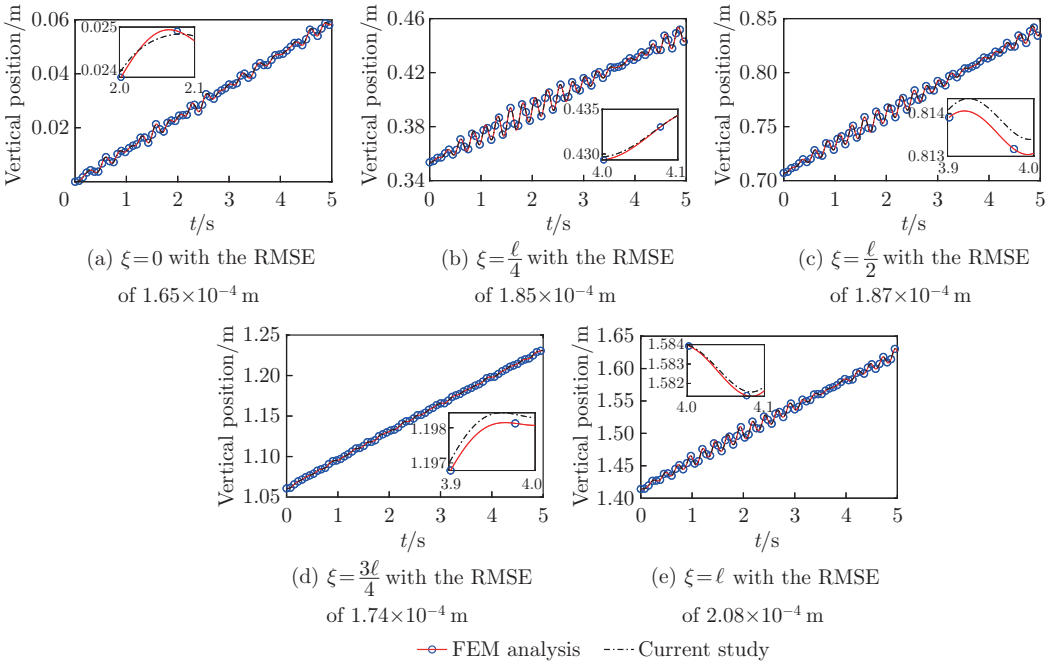

Fig. 7 Time histories of the vertical position of different points of the system (color online)

Specifically, according to Fig. 11(a), the error for the horizontal position is less than 0.08%. In addition, according to Figs. 11(b) and 11(c), the errors for the vertical and angular positions are both maintained below 0.15%.

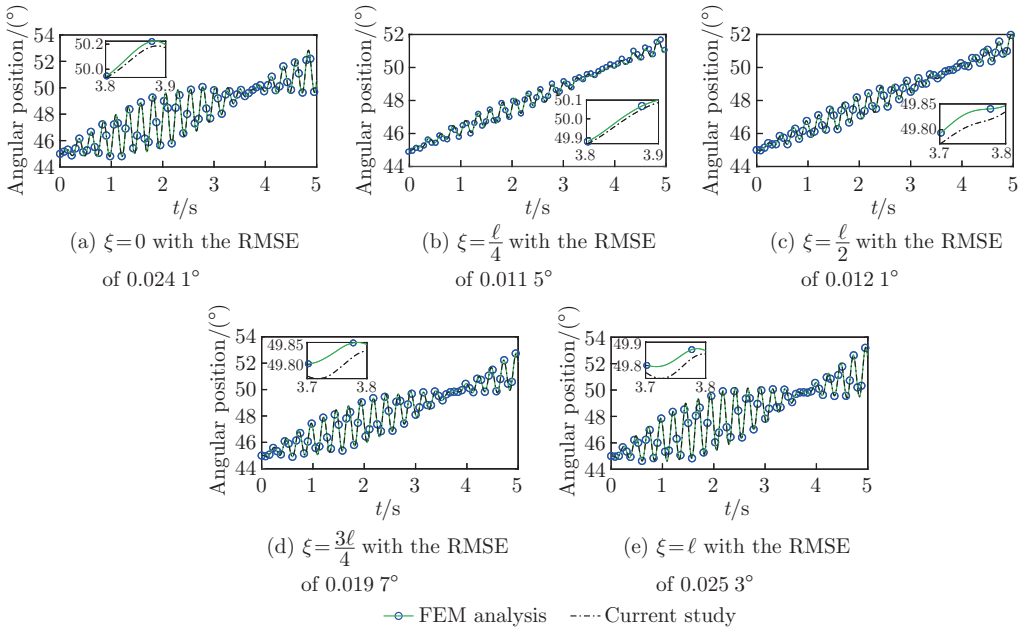

Fig. 8 Time histories of the angular position of different points of the system (color online)

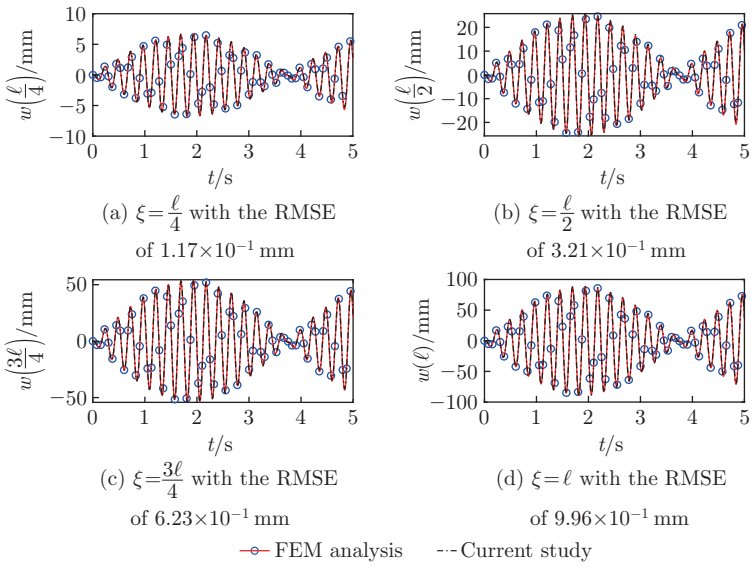

Fig. 9 Time histories of the transverse deformation of different points of the Timoshenko arm (color online)

4.3 Number of assumed mode

To assess the effect of the number of assumed modes $\mathcal{N}$ on the accuracy of the results, a series of simulations with 1 to 7 modes are performed. Figure 12 shows the time histories of the error of horizontal, vertical, and angular positions of $\xi = \frac{\ell}{4}$, $\xi = \frac{\ell}{2}$, and $\xi = \ell$ with respect to the FEM analysis. According to this figure, the error generally decreases as the number of modes increases. To achieve an error less than 3% in all situations, it is sufficient to use only the first three assumed modes. In fact, by solving a third-order problem based on the proposed

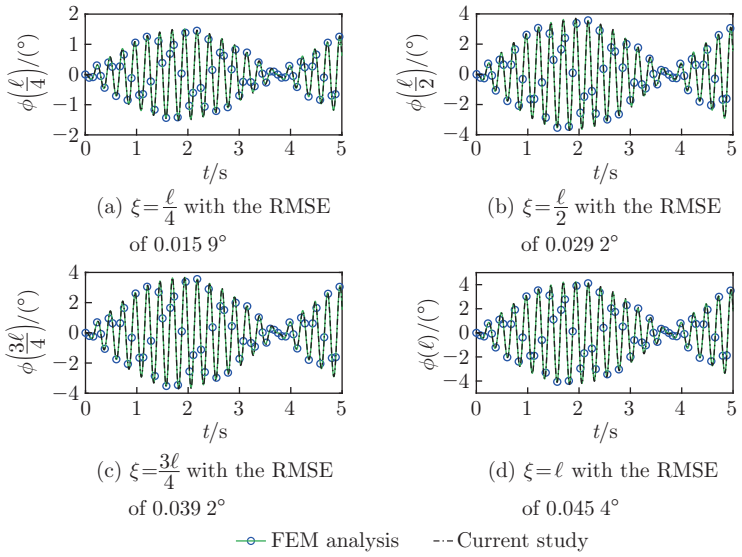

Fig. 10 Time histories of rotation of arm sections due to bending (color online)

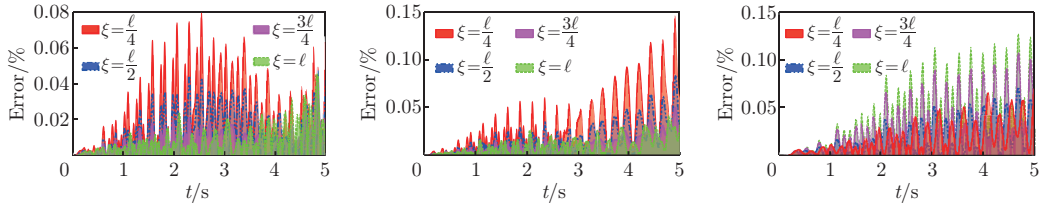

Fig. 11 Error analyses of the horizontal, vertical, and angular positions of different points of the system with respect to the FEM analysis (color online)

model, it is possible to predict the elastic behavior of the system with an error less than 3% when compared with a 200th-order finite element model.

4.4 Study on rigid body dynamics assumption

As discussed in Remark 4, despite the rigidity of the arm in the axial direction, due to the transverse elasticity of the beam, modeling errors can occur when describing the axial reaction concerning Eq. (35). The system response considering Eq. (35) is shown in Fig. 13. The horizontal, vertical, and angular positions of the system at $\xi = 0$ are depicted in Figs. 13(a), 13(b), and 13(c), respectively, while the transverse displacement and rotation of the section due to bending at $\xi = \ell$ are shown in Figs. 13(d) and 13(e), respectively. As shown in the figure, although the use of Eq. (35) for modeling does not seriously affect the angular position and elastic deformations, it results in a significant error in the horizontal and vertical positions of the system.

5 Conclusions

The main objective of this study is to propose an accurate model for a nonlinearly vibrating mobile single-link manipulator with a Timoshenko arm. In this manner, the AMM approach is considered to solve the model after obtaining a hybrid PDE-ODE model of the system using Newton's second law. The natural mode shapes of a clamped Timoshenko beam with an attached tip mass/inertia are used as assumed modes of the nonlinear system to improve the

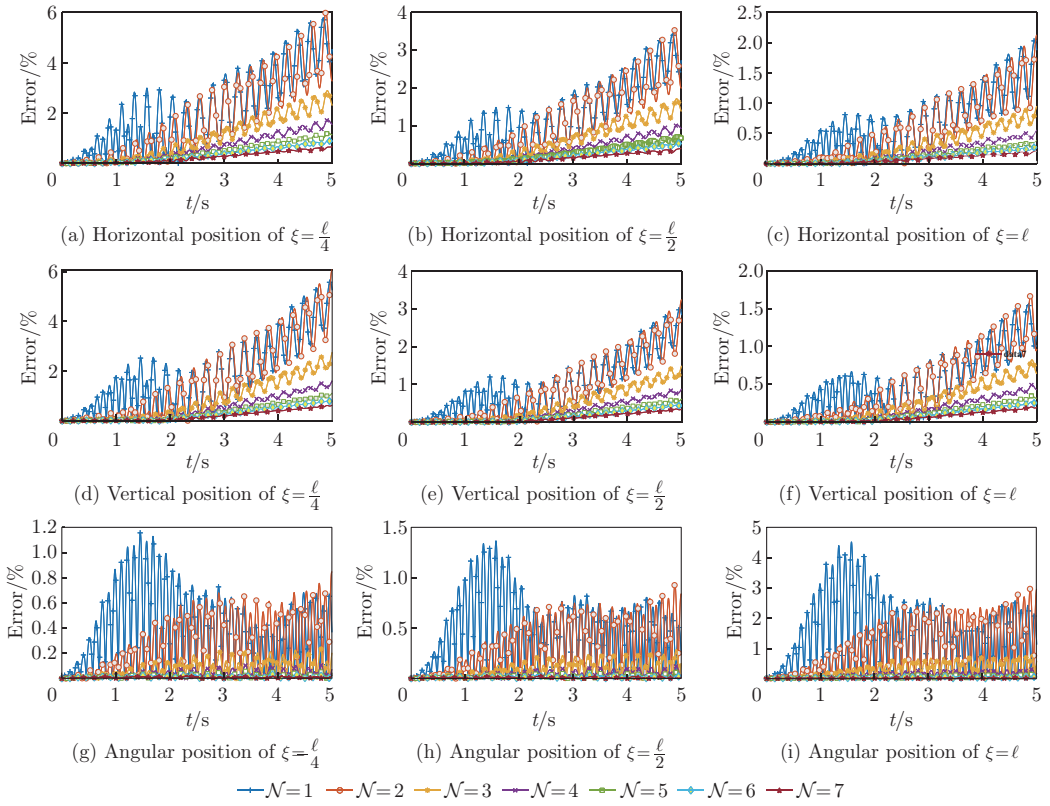

Fig. 12 Time histories of the error of horizontal, vertical, and angular positions of different points of the system (color online)

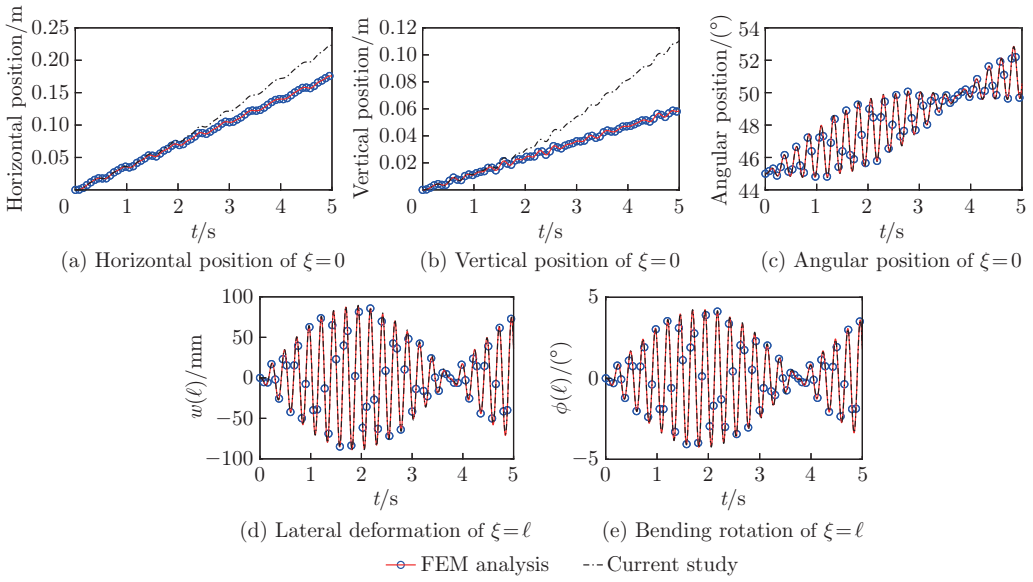

Fig. 13 Effects of the improper rigid body dynamics assumption on the axial direction of the beam (color online)

accuracy. Then, the transient analysis of the system under the action of external excitations is performed to evaluate the validity of the extracted model. The FEM analysis using commercial software is conducted to validate the proposed model, and the results are compared. The results illustrate that a high-accuracy model of the system can be obtained at a lower computational cost compared with the FEM using a limited number of assumed modes. Additionally, the effect of transverse deformations on the axial behavior of the arm is first discussed theoretically and then confirmed using appropriate numerical simulations. Despite the axial rigidity, the rigid body dynamics assumption in the axial direction is not valid, and leads to significant modeling errors.

Conflict of interest The authors declare no conflict of interest.

References

[1] MISHRA, N. and SINGH, S. P. Determination of modes of vibration for accurate modelling of the flexibility effects on dynamics of a two link flexible manipulator. *International Journal of Non-Linear Mechanics*, **141**, 103943 (2022)

[2] WU, D., ENDO, T., and MATSUNO, F. Exponential stability of two Timoshenko arms for grasping and manipulating an object. *International Journal of Control, Automation and Systems*, **19**, 1328–1339 (2021)

[3] LI, C. Nonlocal thermo-electro-mechanical coupling vibrations of axially moving piezoelectric nanobeams. *Mechanics Based Design of Structures and Machines*, **45**(4), 463–478 (2017)

[4] WEI, J., CAO, D., WANG, L., HUANG, H., and HUANG, W. Dynamic modeling and simulation for flexible spacecraft with flexible jointed solar panels. *International Journal of Mechanical Sciences*, **130**, 558–570 (2017)

[5] MENG, D., SHE, Y., XU, W., LU, W., and LIANG, B. Dynamic modeling and vibration characteristics analysis of flexible-link and flexible-joint space manipulator. *Multibody System Dynamics*, **43**, 321–347 (2018)

[6] HOMAEINEZHAD, M. R. and ABBASI GAVARI, M. Feedback control of actuation-constrained moving structure carrying Timoshenko beam. *International Journal of Robust and Nonlinear Control*, **33**(3), 1785–1806 (2023)

[7] MOSLEMI, A. and HOMAEINEZHAD, M. R. Effects of viscoelasticity on the stability and bifurcations of nonlinear energy sinks. *Applied Mathematics and Mechanics* (*English Edition*), **44**(1), 141–158 (2023) https://doi.org/10.1007/s10483-023-2944-9

[8] WANG, Z., WU, W., GÖRGES, D., and LOU, X. Sliding mode vibration control of an Euler-Bernoulli beam with unknown external disturbances. *Nonlinear Dynamics*, **110**, 1393–1404 (2022)

[9] ZHU, K. and CHUNG, J. Vibration and stability analysis of a simply-supported Rayleigh beam with spinning and axial motions. *Applied Mathematical Modelling*, **66**, 362–382 (2019)

[10] SOLDATOS, K. P. and SOPHOCLEOUS, C. On shear deformable beam theories: the frequency and normal mode equations of the homogeneous orthotropic Bickford beam. *Journal of Sound and Vibration*, **242**, 215–245 (2001)

[11] SHAN, J., ZHUANG, C., and LOONG, C. N. Parametric identification of Timoshenko-beam model for shear-wall structures using monitoring data. *Mechanical Systems and Signal Processing*, **189**, 110100 (2023)

[12] LEE, T. S. and ALANDOLI, E. A. A critical review of modelling methods for flexible and rigid link manipulators. *Journal of the Brazilian Society of Mechanical Sciences and Engineering*, **42**, 508 (2020)

[13] HUANG, T. C. The effect of rotatory inertia and of shear deformation on the frequency and normal mode equations of uniform beams with simple end conditions. *Journal of Applied Mechanics*, **28**, 579–584 (1961)

[14] JIN, H., SUI, S., ZHU, C., and LI, C. Axial free vibration of rotating FG piezoelectric nanorods accounting for nonlocal and strain gradient effects. *Journal of Vibration Engineering and Technologies*, **11**(2), 537–549 (2023)

[15] FAN, W. An efficient recursive rotational-coordinate-based formulation of a planar Euler-Bernoulli beam. *Multibody System Dynamics*, **52**, 211–227 (2021)

[16] HE, W., OUYANG, Y., and HONG, J. Vibration control of a flexible robotic manipulator in the presence of input deadzone. *IEEE Transactions on Industrial Informatics*, **13**(1), 48–59 (2017)

[17] ZHAO, Z. and LIU, Z. Finite-time convergence disturbance rejection control for a flexible Timoshenko manipulator. *IEEE/CAA Journal of Automatica Sinica*, **8**, 157 (2021)

[18] SINHA, S. K. Nonlinear dynamic response of a rotating radial Timoshenko beam with periodic pulse loading at the free-end. *International Journal of Non-Linear Mechanics*, **40**(1), 113–149 (2005)

[19] VAKIL, M., SHARBATI, E., VAKIL, A., HEIDARI, F., and FOTOUHI, R. Vibration analysis of a Timoshenko beam on a moving base. *Journal of Vibration and Control*, **21**(6), 1068–1085 (2015)

[20] XING, X. and LIU, J. PDE model-based state-feedback control of constrained moving vehicle-mounted flexible manipulator with prescribed performance. *Journal of Sound and Vibration*, **441**, 126–151 (2019)

[21] LI, L. and LIU, J. Consensus tracking control and vibration suppression for nonlinear mobile flexible manipulator multi-agent systems based on PDE model. *Nonlinear Dynamics*, **111**, 3345–3359 (2023)

[22] XUE, H. and HUANG, J. Dynamic modeling and vibration control of underwater soft-link manipulators undergoing planar motions. *Mechanical Systems and Signal Processing*, **181**, 109540 (2022)

[23] KORAYEM, M. H. and DEHKORDI, S. F. Derivation of motion equation for mobile manipulator with viscoelastic links and revolute-prismatic flexible joints via recursive Gibbs-Appell formulations. *Robotics and Autonomous Systems*, **103**, 175–198 (2018)

[24] KORAYEM, M. H. and DEHKORDI, S. F. Dynamic modeling of flexible cooperative mobile manipulator with revolute-prismatic joints for the purpose of moving common object with closed kinematic chain using the recursive Gibbs-Appell formulation. *Mechanism and Machine Theory*, **137**, 254–279 (2019)

[25] COWPER, G. R. The shear coefficient in Timoshenko's beam theory. *Journal of Applied Mechanics*, **33**(2), 335–340 (1966)

[26] TIMOSHENKO, P. S. P. LXVI. On the correction for shear of the differential equation for transverse vibrations of prismatic bars. *The London, Edinburgh, and Dublin Philosophical Magazine and Journal of Science*, **41**(245), 744–746 (1921)

[27] HAN, S. M., BENAROYA, H., and WEI, T. Dynamics of transversely vibrating beams using four engineering theories. *Journal of Sound and Vibration*, **225**(5), 935–988 (1999)

[28] MEIROVITCH, L. *Analytical Methods in Vibrations*, *Macmillan Series in Applied Mechanics*, 1st ed., Macmillan, New York (1967)